Calculation of nucleon production cross sections for 200 Mev Deuterons

D. Ridikas, W. Mittig

HAL Id: in2p3-01618871

https://hal.in2p3.fr/in2p3-01618871

Submitted on 18 Oct 2017

GANIL

Calculation of Nucleon Production Cross Sections
for 200 MeV Deuterons

D. Ridikas and W. Mittig

GANIL (CEA/DSM-CNRS/IN2P3), BP 5027, F-14076 CAEN Cedex 5, France

SW9725
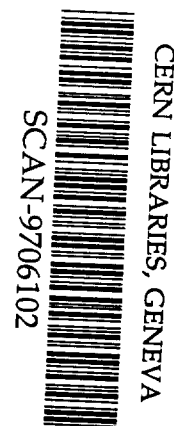
Calculation of Nucleon Production Cross Sections for 200 MeV Deuterons

D. Ridikas and W. Mittig

GANIL (CEA/DSM-CNRS/IN2P3), BP 5027, F-14076 CAEN Cedex 5, France

May 23, 1997

Abstract

We have investigated the differential neutron and proton production cross sections for 200 MeV incident deuterons on thin and thick ^{9}Be, ^{56}Fe and ^{238}U targets using the LAHET code system. The examples of the deuteron beam on different target materials are analysed to determine the differences of converting the energy of the beam into the nucleons produced. Both double differential, energy and angle integrated nuclear production cross sections are presented together with the average nucleon multiplicities per incident deuteron. The calculations may also be useful for estimations of radiation protection using deuteron beams at GANIL.

1 Introduction

The use of neutrons for transmutation of the long-lived radioactive nuclei of nuclear waste to stable or short-lived species has been under consideration already for many years [1]. When an energetic particle hits the target material consisting of heavy nuclei, tens of neutrons might be generated. This is of course, the feature of outermost importance for the so-called subcritical hybrid systems (see [2] and Refs. therein). The interest in neutron production reactions has been recently renewed because they are the basis in the development of powerful neutron sources for various purposes like nuclear energy production and incineration of nuclear waste, material structure analysis, future tritium production, etc. Another interest is related to the possibility of the production exotic nuclei and exotic beams by neutron induced fission. One of the crucial problems in this context is to determine the most efficient way to convert the beam energy into neutrons produced afterwards. Most of the experiments of this type focused both on energy spectra and angular distributions of light particles emitted and on production rate of the residues.

So far only high energy (0.8 − 1.6 GeV) protons hitting a heavy target (uranium, thorium, lead,...) were considered as far as subcritical hybrid systems are concerned [2]. The use of projectiles such as d, α, Li, C, etc. may have competitive features too. Another option is to use light targets as converters to create the neutrons [3]. At GANIL we are undertaking experiments for production of the secondary beams using primary beams ranging from deuterons up to uranium as projectiles. This technique will be applied in a secondary beam facility SPIRAL, actually under construction and scheduled to enter an operation in 1998.

In this report we present and compare benchmark calculations of differential neutron and proton production cross sections made with the LAHET code system [4] for 200 MeV incident deuterons on ^{9}Be, ^{56}Fe and ^{238}U targets. More detailed calculations of production cross sections of nucleons and residual nuclei with the multiplication and attenuation effects in a given target geometry are in progress.

2 Physics models of the LAHET code

Many theories have been formulated to describe preequilibrium phenomena induced by various projectiles. Among them are the internuclear cascade model [5], the quasi-free scattering model [6], the preequilibrium exciton model [7, 8],

1

and hybrid model [9]. These various models have been reasonably successful in accounting for a large body of experimental data. The LAHET code [4] employs the most popular theoretical approach to spallation reactions, namely the internuclear cascade (INC) and evaporation models. As an alternative to the Bertini INC [10], this code contains the INC routines from the ISABEL code. The ISABEL INC model is an extension by Yariv and Fraenkel [11] of the VEGAS code [12]. It has the capability of treating nucleus-nucleus interactions as well as particle-nucleus interactions. It allows for interactions between the particles both of which are excited above the Fermi sea [13]. The nuclear density is represented by up to sixteen steps, rather than three steps as in Bertini INC. It also allows antiproton annihilation [14]. However, antiproton annihilation is not allowed in particle transport problems.

LAHET includes two models of fission induced by high energy interactions: the ORNL model by Alsmiller et al. [15] and the RAL model by Atchison [16] as an optional choice by user; the fission models are employed with the evaporation model of Dresner [17]. The Fermi breakup model [18] has replaced the evaporation model for the disintegration of light nuclei ($A \leq 17$); it treats the deexcitation process as a sequence of simultaneous breakup of the excited nucleus into two or more products each of which may be a stable or unstable nucleus or a nucleon. Any unstable products nucleus is a subject of subsequent breakup. The probability for a given breakup channel is primarily determined from the available phase space with probabilities for two-body channels modified by Coulomb barrier, angular momentum and isospin factors. In the LAHET implementation, only two- and three-body breakup channels are considered.

LAHET also contains the multistage preequilibrium exciton model (MPM) as described in [19]. The MPM is invoked at the completion of the INC, with an initial particle-hole configuration and excitation energy determined by the outcome of the cascade. At each stage in the MPM, the excited nucleus may emit a neutron, proton, deuteron, triton, ^{3}He or alpha; alternatively the nuclear configuration may evolve toward an equilibrium exciton number by increasing the exciton number by one particle-hole pair. The MPM terminates upon reaching the equilibrium exciton numbers; the evaporation model (or the Fermi breakup model for light nuclei) is applied to the residual nucleus with the remaining excitation energy.

LAHET differs from the HETC code [17] in the use of cutoff energies of particles escaping from the nucleus during the internuclear cascade. The default

procedure is to apply a fixed cutoff barrier for neutrons equal to the mean binding energy of one proton and one neutron with respect to the target nucleus; escaping particles with final energy below the cutoff are retained by the nucleus. For protons, the cutoff energy is the maximum of the neutron cutoff energy and a Coulomb barrier.

In additon, we refer the reader to Ref. [4], where the resulting data garnered from running LAHET and subsequent post-processing codes has been compared extensively against experimental data in a multitude of varying target materials, projectile particle type and energy, and geometry.

Finally, we should mention that for ejectile energies $E \leq 20$ MeV the nucleon transport is performed using the MCNP code [20] which is also installed and merged with the LAHET code system here at GANIL [21].

3   General features of energy spectra

The shape of the energy spectra both for neutron and proton production seems to be rather well established as far as proton induced reactions are concerned (see for example [22, 23, 24, 25, 26, 27] and Refs. therein). It is interesting to discuss these spectra a little bit though as they provide a clue to the physics involved.

There is a characteristic peak at large energies (almost the incident energy) which is well seen at forward angles, and which fades out both with increasing scattering angle and the increasing mass number of projectile. Here the pp and pn quasielastic scattering is the important mechanism, i.e. a nucleon is ejected by the incoming proton and leaves the target without further interaction. To be more precise, this quite broad peak contains the unresolved contributions from the isobaric analog transition and the collective strength of Gamow-Teller ($L = 0$) resonance, the spin-flip dipole ($L = 1$), and the quadrupole mode ($L = 2$) resulting from direct one-step process of one-particle-one-hole configuration ($1p - 1h$) spin-isospin excitation of the target nucleus [28].

The spectra show little target specific features too; the absolute cross sections scale as $A^{\alpha(E_{cm})}$, where A is the projectile (and target) mass and E_{cm} stands for a kinetic energy of projectile in the center-of-mass system [22]. If all nucleons are emitted from direct processes without any multiple collisions, then we may assume that the A dependence is determined only by the collision geometry. In this case the expected A dependence of the cross section is given by $A^{5/3}$, since the inclusive yield is proportional to the participant nucleon number (which is

3

proportional to A) multiplied by the geometrical cross section (which is proportional to $A^{2/3}$). As a general trend, $\alpha(E_{cm})$ increases together with the projectile energy. It was found that low-energy protons are more abundantly produced for heavier-mass targets than for lighter-mass targets, presumably because of effects of target fragmentation. Once the projectile is fixed, however, the shape of the high-energy tails does not depend strongly on target mass [23].

At forward angles, the cross section at low energy decreases slowly with increasing energy, while those at high energy decrease exponentially with a steeper slope. Such a spectrum is called *shoulder-arm* shape [22]. The turning point between the shoulder and arm is located at energy close to the peak observed in proton collisions at forward scattering angle. As the scattering angle increases, the position of turning point between the shoulder and arm shifts to smaller energies and the exponential tale becomes steeper.

These characteristics led Serber [29] to propose very early a two-stage picture of the spallation reaction mechanisms, namely a first fast stage in which the incident proton looses part of its energy by individual nucleon-nucleon scattering and a second slow stage in which the remaining target excitation energy is released by evaporation. The component of the nucleon spectra extending between the evaporation bump and the quasielastic peak mentioned above is due to multiple collisions in this description.

It is interesting to note that the shapes of neutron cross sections as functions of energy are similar to the ones of protons at the same energy and for the same target. Therefore, the phenomenological parametrization of Kalbach [30] is often used to describe continuum angular distributions for various projectiles and ejectiles over a large range of incident energies. The cross section for a purely direct reaction, which should be the dominant component in this process, is given by

$$\frac{d^2\sigma}{d\Omega dE} = \sigma_D \frac{\eta}{\sinh\eta} exp(\eta cos\theta),\qquad(1)$$

where θ is the center-of-mass scattering angle, and $4\pi\sigma_D$ is the angle integrated cross section, which might be determined by normalizing the calculated values to the experimental data. Below the incident energy of $E_a = 130$ MeV of the projectile a, the slope parameter η is expressed as

$$\eta = \alpha e_b + \beta e_b^3 + \gamma e_b^4\qquad(2)$$

4

with $e_b = E_b + S_b$. Here E_b is the emission energy of the outgoing particle b and S_b stands for its separation energy in the compound-nuclear system. The constants α, β and γ are listed by Kalbach [30].

4 Results and discussion

Our calculations were performed to produce results which could directly compare the (d, xn) and (d, xp) reactions on different target materials with 200 MeV incident deuterons. In Fig. 1 double differential neutron (on the left) and proton (on the right) production cross sections are plotted as functions of the energy of the ejected nucleon. In general, all the features mentioned in Section 3 are present for both neutron and proton energy spectra.

The characteristic peak at the forward scattering angle is situated nearly at 100 MeV, i.e. the incident energy per nucleon. These energetic nucleons appear due to a direct deuteron breakup on the target nucleus and quasielastic scattering of nucleons followed afterwards. The *shoulder-arm* shape is also clearly exhibited as long as the scattering angle increases. For ejectile energies larger than 10 MeV the shapes of neutron and proton spectra are almost identical for the same target material (compare for example the results with the ^{9}Be target). Only in the case of ^{238}U the (d, xn) cross sections have slightly higher values, which we believe occur due to increased N/P ratio (for ^{238}U it is 1.59, while ^{9}Be has 1.25). This difference appears also for ^{56}Fe but at lower energies. For energies lower than 5 MeV, where most of the particles are produced by the evaporation stage, proton production spectra sharply decrease at all scattering angles both for ^{56}Fe and ^{238}U if compared with corresponding (d, xn) curves (see Fig. 1). On the other hand, only small difference is seen in the case of the ^{9}Be target. This interesting phenomenon is even better seen from Fig. 2, where angle integrated differential cross sections are presented.

It is important to note that the nucleon spectra can be split in a low energy component due to evaporation and high energy component due to the INC stage. A close examination reveals [31] that taking the INC contribution alone for nucleon energies larger than 15 MeV and the evaporation contribution alone for less than 15 MeV would give essentially the same result as the one obtained with the full calculation. Of course, the separation between INC and evaporation is somewhat artificial and model dependent. The necessity to flip to evaporation model is not just a matter of convienience (running the cascade is a time-consuming pro-
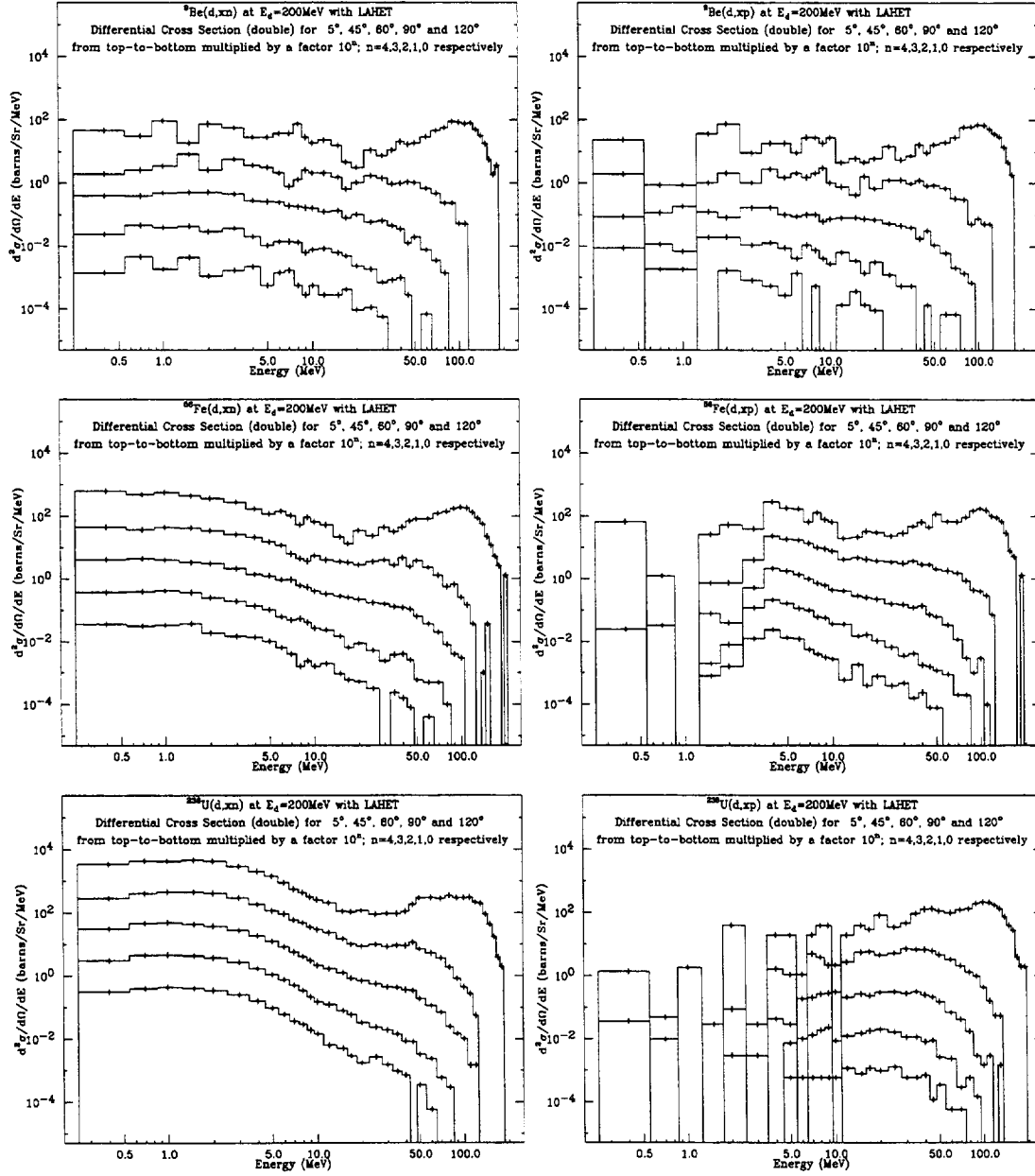
Figure 1: Calculated energy spectra for the nucleon production reactions (d, xn) (on the left) and (d, xp) (on the right) for 200 MeV incident deuterons on thin ^{9}Be, ^{56}Fe and ^{238}U targets for various scattering angles. Results are multiplied by the factors as indicated for graphical display.
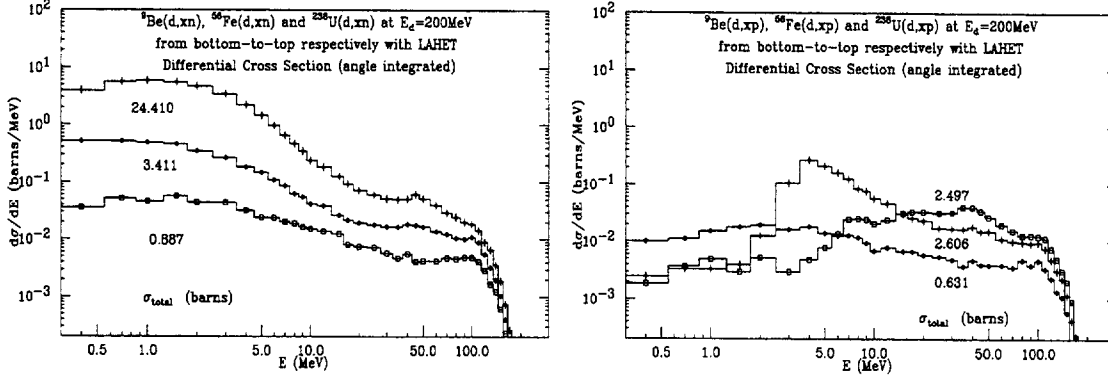
Figure 2: Calculated angle integrated energy spectra for the nucleon production reactions (d, xn) (on the left) and (d, xp) (on the right) for 200 MeV incident deuterons on thin ^{9}Be, ^{56}Fe and ^{238}U. Corresponding total production cross sections σ_{total} are also given.

cess) but it is dictated by the fact that the evaporation process involves structure effects (shell effects and configuration mixing) that are not taken into account by the cascade which embodies average single particle properties only. Usually, a criterion is chosen to stop the cascade process at some stage, which in the LAHET code pertains to the possible largest kinetic energy of the nucleons (related to binding energy and Coulomb barrier for protons) remaining in the target. This knowledge may be helpful understanding the behaviour of proton spectrum at low energies presented in Fig. 2. With increasing mass of target nucleus the INC contribution becomes dominating for proton production spectra, while for neutrons the evaporation process is the most important one. Here we refer the reader to Table 1, where both evaporation and INC contributions to the total cross section are given explicitly. In the case of ^{56}Fe, both INC and evaporation

	^{9}Be		^{56}Fe		^{238}U	
Cross section, (b)	prot.	neut.	prot.	neut.	prot.	neut.
σ_{evap}	0.087	0.191	1.061	1.707	0.107	19.122
σ_{INC}	0.544	0.696	1.545	1.704	2.390	5.288
σ_{total}	0.631	0.887	2.606	3.411	2.497	24.410

Table 1: Contribution of two different processes to the total proton and neutron production cross section σ_{total} from the INC stage and the evaporation stage given by σ_{INC} and σ_{evap} respectively.

7

are of comparable importance, probably because of the high binding energy of this nucleus. It might be the reason of the quite pronounced peak approximately at 4 MeV well seen on the right of Fig. 2.

Unfortunately, almost all experimental data available for proton production cross sections do not contain spectra for low energies. Usually they start at $10 - 20$ MeV because of technical difficulties when the high energy spectrum is measured in the same experimental setup.

The absolute values of the angle integrated spectra for (d, xn) (on the left of Fig. 2) follow a target mass dependence $d\sigma/dE \sim A^\alpha$ with $\alpha \approx 0.84$ for forward directions, which is in qualitative support of a nucleon-nucleon collision picture, i.e. they exhibit a proportionality to the geometrical cross section ($\alpha \approx 0.67$). The same is to be said about the (d, xp) reaction for proton energies larger than 30 MeV (on the right of Fig. 2). At lower energies proton production cross sections show quite interesting behaviour, in particular for the ^{56}Fe target case, what, as we believe, is related to the Coulomb barrier for proton emission. Quite sharp decline in the cross section is predicted with decreasing energy of the emitted protons both for ^{56}Fe and for ^{238}U. For ^{9}Be the Coulomb barrier is much smaller, therefore the enery dependence of the cross section looks very similar to the one of neutrons. On the other hand, we want to mention in this connection that this
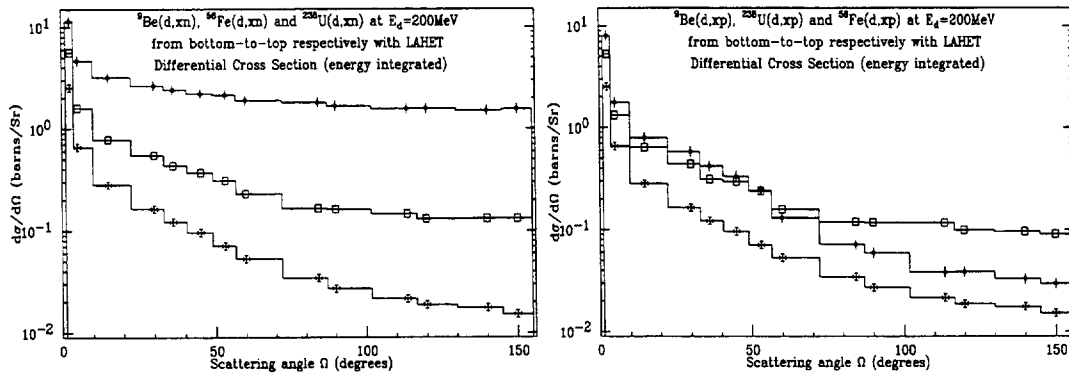

Figure 3: Calculated energy integrated energy spectra for the nucleon production reactions (d, xn) (on the left) and (d, xp) (on the right) for 200 MeV incident deuterons on thin ^{9}Be, ^{56}Fe and ^{238}U targets.

phenomenon could easily be checked experimentally if proton production spectra are measured at least starting with energies of $1 - 2$ MeV. The experiment for the (d, xp) and (d, xn) reaction at 200 MeV incident deuterons on ^{9}Be and ^{238}U targets is planned in June 1997 at SATURNE experimental facility (Saclay).

8

In addition to energy distributions, in Fig. 3 we present predicted angular distributions. It is clearly seen that most of the protons after the breakup are ejected at forward angles (on the right). The cross section decreases rapidly with the scattering angle as shown in Fig. 3, and this feature is target-independent. On the other hand, the (d, xn) reaction shows a some-what different angular dependence; the cross section decreases considerably with the angle in the case of ^{9}Be and ^{56}Fe, while for the ^{238}U target neutrons are emitted in the entire scattering angle range (see on the left of Fig. 3). Here multiple nucleon scattering and secondary neutron production during the evaporation stage contribute mostly (see also Table 1). This observed difference might be very important in further investigations on neutron production spectra within subcritical hybrid systems, where the use of light or heavy targets is still an open question. One could think of the combined system, for example, with a light target as a converter in order to create the neutrons (which as we have shown are mostly emitted at forward angles for light targets) and a heavy target (placed right after the light target) to increase the neutron flux further. We have made some preliminary calculations for neutron multiplicities from the (n, xn) reaction on a thick ^{238}U target at

	^{9}Be		^{56}Fe		^{238}U	
Energy range, (MeV)	$\langle M_p \rangle$	$\langle M_n \rangle$	$\langle M_p \rangle$	$\langle M_n \rangle$	$\langle M_p \rangle$	$\langle M_n \rangle$
≥ 50.0	0.313	0.318	0.144	0.151	0.073	0.117
≥ 25.0	0.495	0.664	0.271	0.322	0.158	0.279
≥ 10.0	0.679	1.068	0.421	0.506	0.194	0.548
≥ 0.0	0.746	1.538	0.637	1.112	0.211	2.650

Table 2: Predicted proton $\langle M_p \rangle$ and neutron $\langle M_n \rangle$ multiplicities in units of nucleons emitted per incident deuteron for different thick target materials and different energy regions.

different incident energies. The following average numbers were obtained: 10.6, 8.7, 6.8 and 4.2 neutrons per source neutron at the incident energies of 100, 75, 50 and 25 MeV respectively.

Finally in Fig. 4 we show calculations of nucleon yield from thick targets. As a matter of fact, all of the graphs presented here are similar to these displayed in Fig. 2, where angle integrated nucleon production cross sections are plotted. Again for energies larger than 30 MeV the weight of protons and neutrons emitted per incident deuteron is almost the same, only for ^{238}U slightly more neutrons are
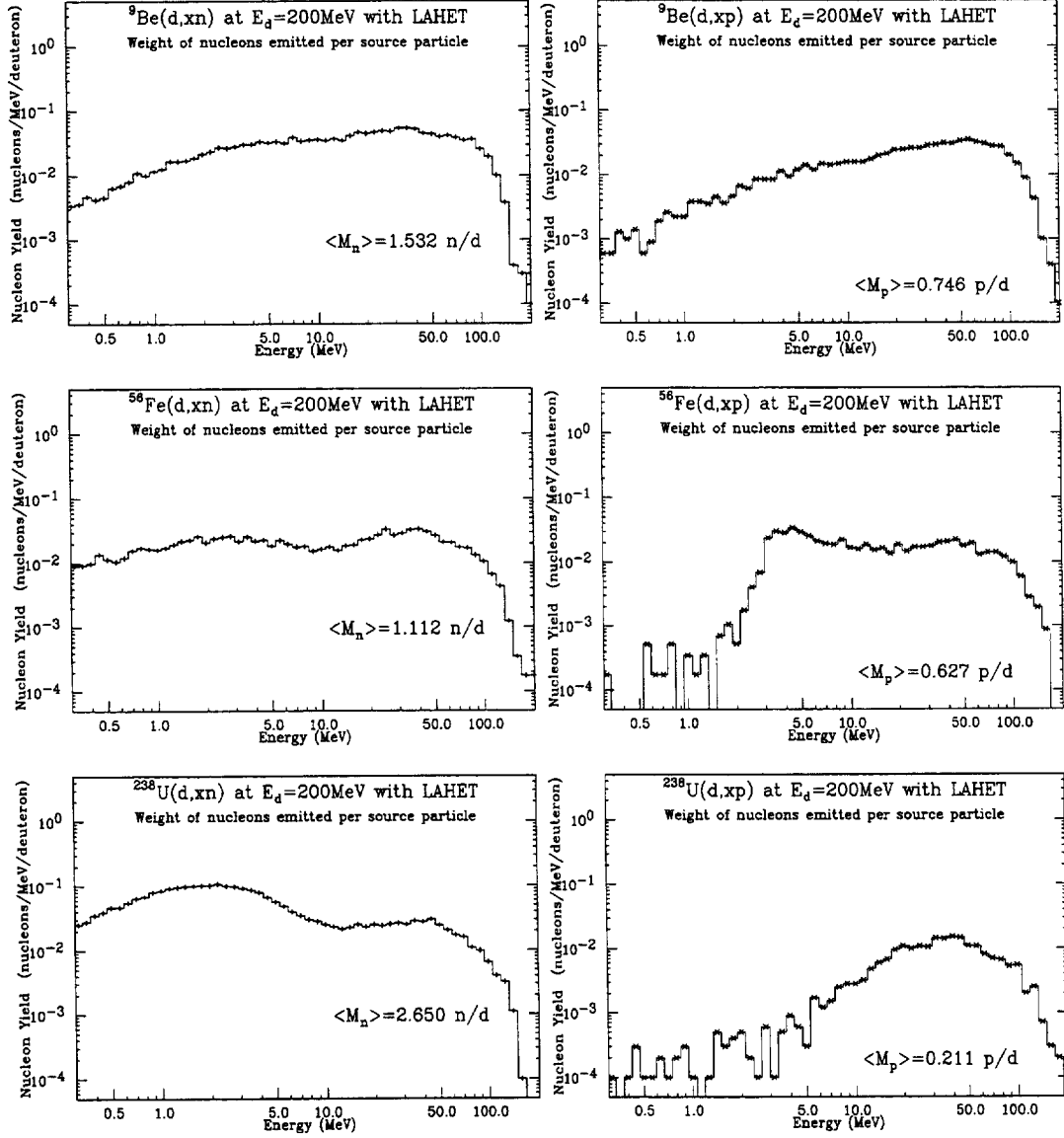
Figure 4: Nucleon emission probabilities per incident deuteron as a function of energy for the reactions of (d, xn) (on the left) and (d, xp) (on the right) with 200 MeV incident deuterons on thick ^{9}Be, ^{56}Fe and ^{238}U targets. The corresponding energy integrated numbers of nucleons produced per incident deuteron are given too.

10

produced in this energy region. It is important to note though at this stage that light targets produce much more energetic neutrons than the heavy ones. The reader may find useful numbers in Table 2. This is, of course, directly related to the different contributions by the INC and evaporation processes as shown in Table 1. The proton production (on the right of Fig. 4) decreases much faster with decreasing energy as compared to neutrons (on the left of Fig. 4). This is again related to the Coulomb barrier for proton emission as we already discussed above.

5 Conclusions

The investigation of spallation reactions induced by 200 MeV deuterons has provided the differential neutron and proton production cross sections for thin ^{9}Be, ^{56}Fe and ^{238}U targets. Differences and common features of the energy and angular spectra were discussed along with their interpretation within the LAHET code system. We found that for light and heavy targets angular distributions of neutrons exhibit different behaviour; neutrons from heavy target are emitted in the entire region of scattering angle, while for light targets most of the neutrons are produced at forward angles. This phenomenon together with multiplicity distributions of nucleons from thick targets also presented in this report provide us with useful characteristics for the choice of heavy or light target material as far as subcritical hybrid systems are concerned. The ^{9}Be target produces 3 times more high energy neutrons than the ^{238}U target. The possibility of a subsequent multiplication of these neutrons in a fissile material render the combination of a light target material with the medium energy deuterons competitive with a heavy target material and high energy protons both for hybrid systems and for the production of radioactive beams by fission. Extension of these investigations to more systematic studies with different projectiles, different target materials, a wider range of incident energy and a more realistic reaction geometry is desirable. Consequently, these findings should ultimately be confirmed by new experimental data.

6 Acknowledgments

References

[1] L.C. Hebel *et al.*, Rev. Mod. Phys. **50** (1978) 1

[2] C.D.Bowman *et al.*, Nucl. Instr. & Meth. **A 320** (1992), 336

[3] Concept for Advanced Exotic Beam Facility Based on ATLAS, Argonne National Laboratory, (February 1995)

[4] R.E. Prael and H. Lichtenstein, "User Guide to LCS: The LAHET Code System," Los Alamos National Laboratory Report LA-UR-89-3014, (September 1989)

[5] H.W. Bertini, Phys. Rev. **131** (1963), 1801

[6] A. Mignerey *et al.*, Nucl. Phys. **A 273** (1976), 125

[7] J.J. Griffin, Phys. Rev. Lett. **17** (1966), 478

[8] M. Blann, Phys. Rev. Lett. **21** (1968), 1357

[9] M. Blann, Phys. Rev. Lett. **28** (1972), 757

[10] H.W. Bertini, Phys. Rev. **188** (1969), 1711

[11] Y. Yariv and Z. Fraenkel, Phys. Rev. **C 20** (1979), 2227

[12] K. Chen *et al.*, Phys. Rev. **166** (1968), 949

[13] Y. Yariv and Z. Fraenkel, Phys. Rev. **C 24** (1981), 488

[14] M.R. Clover, R.M. DeVries, N.J. DiGiacomo and Y. Yariv, Phys. Rev. **C 26** (1982), 2138

[15] J. Barish *et al.*, ORNL/TM-7882, Oak Ridge National Laboratory (July 1981)

[16] F. Atchison, "Spallation and Fission in Heavy Metal Nuclei under Medium Energy Proton Bombardment" in "Targets for Neutron Beam Spallation Sources", Jül-Conf-34, Kernforschungsanlage Jülich GmbH (January 1980)

[17] L. Dresner, ORNL/TM-196, Oak Ridge National Laboratory (April 1962)

[18] D.J. Brenner, R.E. Prael, J.F. Discello and M. Zaider, "Improved Calculations of Energy Depostion from Fast Neutrons", in Proceedings Fourth Symposium on Neutron Dosimetry, EUR-7448, Munich-Neuherberg (1981)

[19] R.E. Prael and M. Bozoian, LA-UR-88-3238, Los Alamos National Laboratory (September 1988)

[20] Group X-6, "A General Monte Carlo Code for Neutron and Photon Transport", LA-7396-M, Los Alamos National Laboratory (April 1981)

[21] More detailed information can be provided by one of the authors (D.R.) of this manuscript if requested by E-mail ⟨ridikas@ganil.fr⟩

[22] S. Nagamiya et al., Phys. Rev. C 24 (1981), 971

[23] S. Stamer et al., Phys. Rev. C 47 (1993), 1647

[24] W. Scobel et al., Phys. Rev. C 41 (1990), 2010

[25] A.A. Cowley et al., Phys. Rev. C 43 (1991), 678

[26] S.V. Förtsch et al., Phys. Rev. C 43 (1991), 691

[27] M. Trabandt et al., Phys. Rev. C 39 (1989), 452

[28] F. Osterfeld, D. Cha and J. Speth, Phys. Rev. C 31 (1985), 372

[29] R. Serber, Phys. Rev. 72 (1947), 1114

[30] C. Kalbach, Phys. Rev. C 37 (1988), 2350

[31] J. Cugnon, C. Volant and S. Vuillier, DAPNIA/SPhN-97-01, CEA/Saclay DSM (January 1997)

13